Branislav M. Notaroš

Polarimetric Weather Radar

Overview of principles and applications.

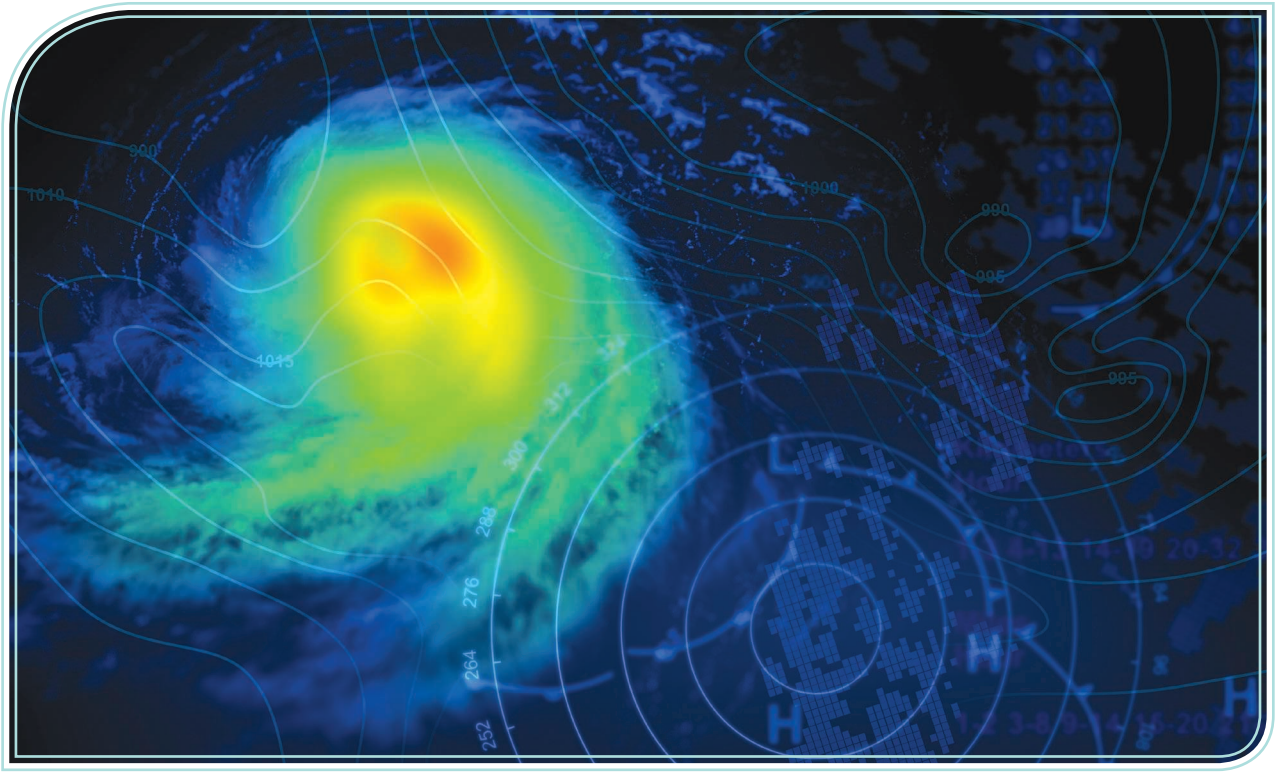

We introduce radar polarimetry, which generally is a less widely known concept of radar engineering, and explain the principles and applications of polarimetric Doppler weather radars. For example, a polarimetric radar can distinguish among precipitation particles of different shapes, compositions, and orientations. A relatively simple electromagnetic idea resulted in the 2012 upgrade of the National Weather Service (NWS) network of 160 high-resolution Doppler weather radars in the United States, with dual-polarization technology. We describe the details of the Colorado State University (CSU)–CHILL research radar, featuring exceptional polarization purity and dual-frequency operation, and its setup and role in winter field experiments in Colorado.

We discuss several illustrative examples of polarimetric weather radar operations and observations and scattering calculations at different frequencies and in various climates. Radar signatures are analyzed in relation to images and measurements by optical instrumentation on the ground. We present three distinct Colorado snowfall cases with fascinating polarimetric signatures at the S band and a rain event with C-band polarimetric scattering computations and measurements by the Advanced Radar for Meteorological and Operational Research (ARMOR),

Digital Object Identifier 10.1109/MAP.2022.3143442
Date of current version: 16 February 2022

in Alabama. Polarimetric weather radar observations are crucial for understanding microphysical properties of precipitation and developing and using numerical models for forecasting and climate projections.

INTRODUCTION

Radar has been used for the remote sensing of the atmosphere, that is, for measurements of electromagnetic scattering from precipitation particles, practically since World War II [1]. Radar meteorology has dramatically advanced based on multiple major scientific and engineering achievements and their synergies. A principal goal of weather radar observations is to relate the characteristics of measured scattered electromagnetic waves and fields to the microphysical properties of rain, snow, and hail particles [2]. This is essential for numerical models for weather forecasting and regional climate modeling and simulations [3].

The principle of Doppler radar has found massive application in weather radar operations and observations since the 1960s [4], [5]. This article focuses on a less widely known concept, that of radar polarimetry, and more recent technology, that of dual polarization, or polarimetric weather radar [5]–[10]. Such a radar transmits well-defined horizontally and vertically polarized electromagnetic waves or horizontal and vertical electric field components and measures the horizontal and vertical components of the scattered field. This produces the 2×2 scattering matrix, which relates the two orthogonal components of the scattered electric field to those of the incident field [11]. The polarimetric scattering properties of precipitation particles open a whole new level of analysis and information about the particles' geometrical and microphysical properties as well as an understanding of cloud processes and the resulting precipitation production and snow and water accumulation [6]–[34].

For example, a polarimetric weather radar can distinguish among particles of different shapes, compositions, and orientations (e.g., rain versus hail, rain versus snow, and snow aggregates versus pristine crystal snowflakes) even in the Rayleigh regime, including at the S band (3 GHz), which is the frequency of operation of all NWS weather radars in the United States. At the S band, precipitation particles are electrically small (much smaller in any linear dimension than the radar wavelength, which is 10 cm in free space), and electromagnetic scattering from such objects undergoes the Rayleigh regime. The "rule of thumb" criterion for Rayleigh precipitation scattering is frequencies less than 10 GHz, with a more precise judgment about the applicability of Rayleigh theory to the scattering from precipitation particles needing information on the size and composition of specific particles and precipitation [5], [35], [36]. Note that the dielectric constant is an important factor in determining whether this approximation is valid. Moreover, polarimetric radar is used for studying severe convective weather, such as tornadic supercells [37], [38].

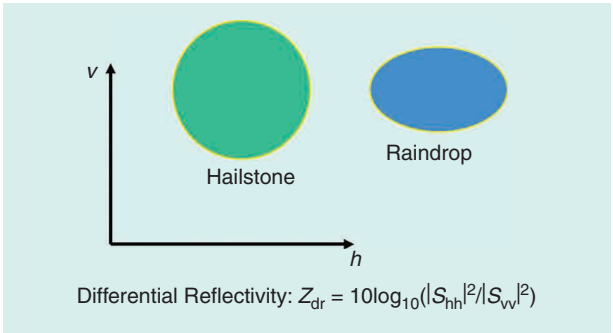

FIGURE 1. A sketch illustrating, more conceptually than quantitatively, a rationale for using polarimetric weather radar: two precipitation particles of varying shapes and orientations have noticeably varying differential reflectivities (Z_{dr}) observed by a polarimetric, or dual-polarization (h and v), radar, whereas reflectivities (Z) measured by a standard (e.g., horizontally polarized) Doppler weather radar do not provide enough information to distinguish between the two shapes/orientations (hailstone and raindrop) [43].

Polarization diversity may include using any pair of "orthogonal" polarizations, including right- and left-hand circular ones [39]. Indeed, circularly polarized Doppler radars have been used in radar meteorology [40], especially in early stages of weather radar polarimetry [9], [41], as well as in nonmeteorological applications [42]. Here, only radar measurements based on linear orthogonal polarization—horizontally and vertically polarized radiation—are considered as a prevailing concept in radar meteorology [5]–[9]. This includes polarimetry with transmitted and received elliptically polarized waves with known and measured horizontal and vertical components [9].

RADAR POLARIMETRY: NEED AND PRINCIPLES

Precipitation particles generally have nonspherical shapes; however, if a conventional (single-polarization) radar is used, the measurements do not provide useful information about the shape and orientations of the particles, namely, that information is ambiguous. Indeed, based on the radar cross section and (single-polarization) reflectivity (Z) [6] (at the horizontal or vertical polarization of the incident electric field), we cannot distinguish among the contributions to Z from the electrical size, shape, and orientation, respectively, of precipitation particles. Hence, a weather radar measuring Z is unable to distinguish scattering from, for example, hailstones and raindrops, as illustrated in Figure 1, assuming the same electrical size [43].

However, in dual-polarization (h- and v-) operation, a polarimetric radar is used to measure the differential reflectivity, Z_{dr}, of precipitation, expressing how the reflectivity at horizontal polarization differs from that at vertical polarization [44]. Specifically, Z_{dr} is obtained as $Z_{dr} = 10\log_{10}(|S_{hh}|^2/|S_{vv}|^2)$, with h and v referring to a horizontally and vertically polarized electromagnetic wave (its electric field vector), respectively, and S_{hh}, S_{hv}, S_{vh}, and S_{vv} being the elements of the 2×2 scattering matrix, relating E_h and E_v components of the scattered electric field to those of the incident field [6]. The two indices on the matrix elements convey the polarization states of the transmitted and received radiation. A polarimetric weather radar thus provides additional information about the shape and orientation of particles. Namely, the Z_{dr} of the hailstone and that of the raindrop in Figure 1 are different, and so are the Z_{dr} values of snowflakes of different shapes.

Another important polarimetric radar measurable is the linear depolarization ratio (LDR), $\mathrm{LDR} = 10\log_{10}(|S_{vh}|^2/|S_{hh}|^2)$, and the full set of the most frequently used polarimetric radar variables are Z_h (horizontal reflectivity), Z_{dr}, LDR, K_{dp} (specific differential phase), and ρ_{hv} (copolar correlation coefficient) [6], [53]. Many other polarimetric variables have been measured and calculated, for example, the specific differential attenuation, A_{dp}, relating the forward scattering amplitude at horizontal and vertical polarizations, used, for instance, to distinguish among large rain drops and melting hail as observed by a C-band radar in intense storms [14]. Note that for a sphere, or a spherical approximation (equivalent sphere with the same volume) of a precipitation particle, $Z_{dr} = 0$ dB, and $\mathrm{LDR} \to -\infty(\mathrm{dB})$.

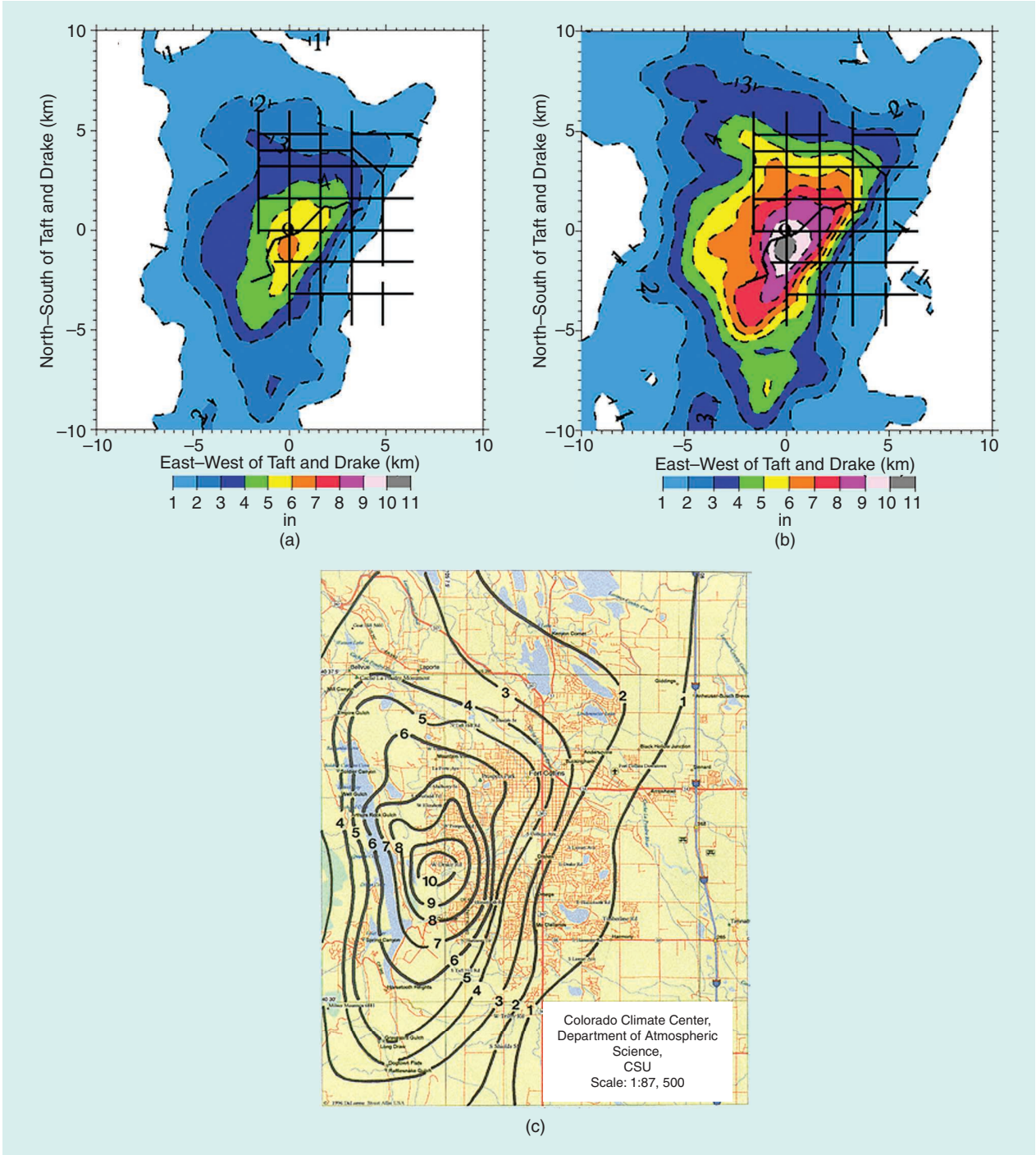

FIGURE 2. A "historical" example of the importance of polarimetric (Figure 1) weather radar operation: radar-based estimation of the rain rate (accumulation) observed by the CSU–CHILL radar operating in (a) the standard (single-polarization) radar regime (NWS WSR-88D radars at the time) and (b) the dual-polarization regime (a unique CSU–CHILL research radar ability at the time); and (c) the precipitation gauge survey of rainfall across Fort Collins on 28 July 1997 [43], [45].

STRIKING HISTORICAL EXAMPLE: FORT COLLINS FLOOD

As a striking "historical" example of the importance of polarimetric weather radar operation, Figure 2 shows the radar-based estimation of the rain rate (accumulation) and a precipitation gauge survey of rainfall for the city of Fort Collins, Colorado, on 28 July 1997, during the infamous Fort Collins Flood. This was a flash flood, where a heavy rain turned ankle-deep Spring Creek flowing through central Fort Collins into a deadly river. During the event, "the water reached over heads, its strong current carried cars from roads and pulled people from their doorsteps or out of the grasp of loved ones" [45], causing five fatalities and huge material damage in the city and on the CSU campus, including the newly constructed university library.

This event produced heavy cumulative rainfall from lots of small raindrops, an atypical situation for Colorado, where fewer, larger drops constitute a more common situation, namely, where drops form by the melting of hail and graupel particles [43]. This could not be observed by a standard (single-polarization) weather radar [NWS Weather Surveillance Radars-1988 Doppler (WSR-88D) at the time] but only with a polarimetric radar (CSU–CHILL research radar), as evident in Figure 2, where a polarimetrically tuned reflectivity–rain rate (Z–R) power law compared well with the gauge-measured rainfall across the city, while a WSR-88D standard Z–R grossly underestimated the accumulation. Specifically, small raindrops are spherical, whereas larger ones become oblate as in Figure 1 (actually, rather flattened on the bottom), and such nonspherical shapes, in turn, are distinguishable by a polarimetric radar. One can speculate that if the NWS had dual-polarization radar capability in its network in 1997, more accurate radar-based precipitation estimation could have provided a flash flood warning that could have saved the lost lives and prevented some of the property damage in the Fort Collins Flood.

NEXRAD NETWORK OF 160 POLARIMETRIC DOPPLER WEATHER RADARS

Prof. V.N. Bringi, coprincipal investigator of the Multi-Angle Snowflake Camera and Radar (MASCRAD) project and a pioneer of polarimetric radar meteorology [6], [44], "spent decades working with what he describes as a relatively simple idea to perfect the complex technology and to convince experimental radar meteorologists that it could be used in operational forecasting. His efforts paid off and his legacy was written when the NWS announced in 2011 that it would be upgrading its nationwide network of 159 Doppler weather radars with dual-polarization technology. The National Severe Storms Laboratory states that the potential benefits with dual polarization will be as significant as the nationwide upgrade to Doppler radar in the 1980s" [46].

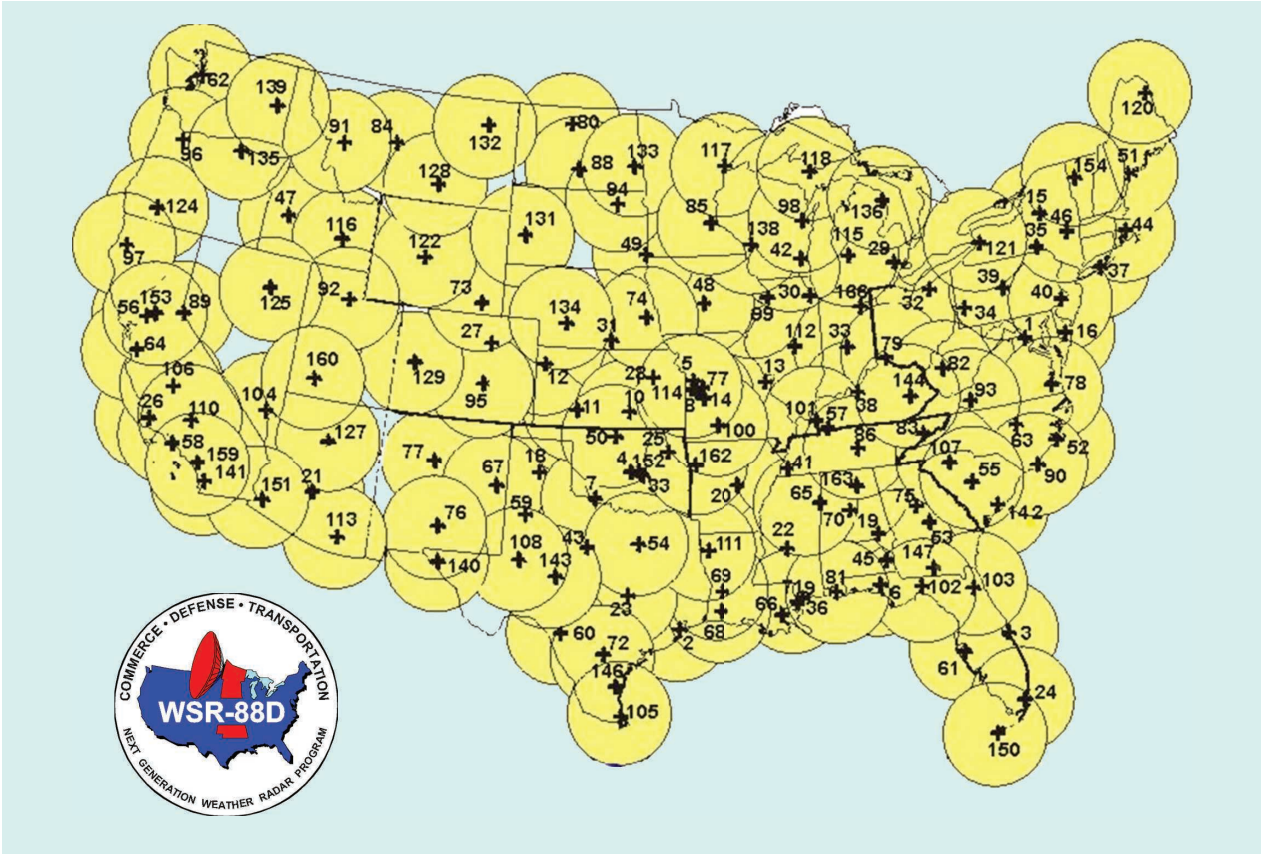

FIGURE 3. The Next-Generation Radar (NEXRAD) network of 160 high-resolution, S-band Doppler weather radars operated by the NWS and National Oceanic and Atmospheric Administration Radar Operations Center, Norman, Oklahoma. In 2012, the NWS upgraded all the NEXRAD WSR-88D radars with dual-polarization technology (see Figures 1 and 2). (Source: NWS; public domain.)

Figure 3 describes the upgraded NWS network of currently 160 high-resolution, S-band polarimetric Doppler weather radars. Radar polarimetry plays an absolutely essential role in weather research and meteorology. Indeed, polarimetric radar signatures in rain, snow, and hail storms with widely differing precipitation particle classes, shapes, sizes, and compositions are distinct and fascinating as well as extremely useful [12]–[34].

DUAL-FREQUENCY, DUAL-POLARIZATION CSU–CHILL RESEARCH RADAR

The CSU–CHILL radar (Figure 4) is a two-transmitter, two-receiver, S-band dual-polarization system. Interestingly, the name of the radar (CHILL) was derived from "CHicago ILLinois radar" in 1970 when the radar was first assembled, and it was kept the same after the facility was moved from Illinois to Colorado, in 1990. The current radar antenna is an 8.5-m, dual-offset Gregorian reflector system [Figure 4(a)] with exceptional polarization purity and very low side lobes (less than –35 dB) in any direction. The radar can measure LDR levels as low as –40 to –43 dB [47]. The antenna is housed inside an inflatable radome, shown in Figure 4(b). Another unique feature of the CSU–CHILL radar is its ability to collect dual-polarization data while operating in dual-frequency mode, with the same antenna reflector system [48]. This is enabled by a two-frequency, two-polarization antenna feed, presented in Figure 4(c), which enables radar operation at the S (3 GHz) and X (9 GHz) bands, either at one frequency or simultaneously at both frequencies. With the same reflector system at both frequencies, the main (3-dB) beamwidth of the antenna comes out to 1° at 3 GHz and 0.33° at 9 GHz, as depicted in Figure 5.

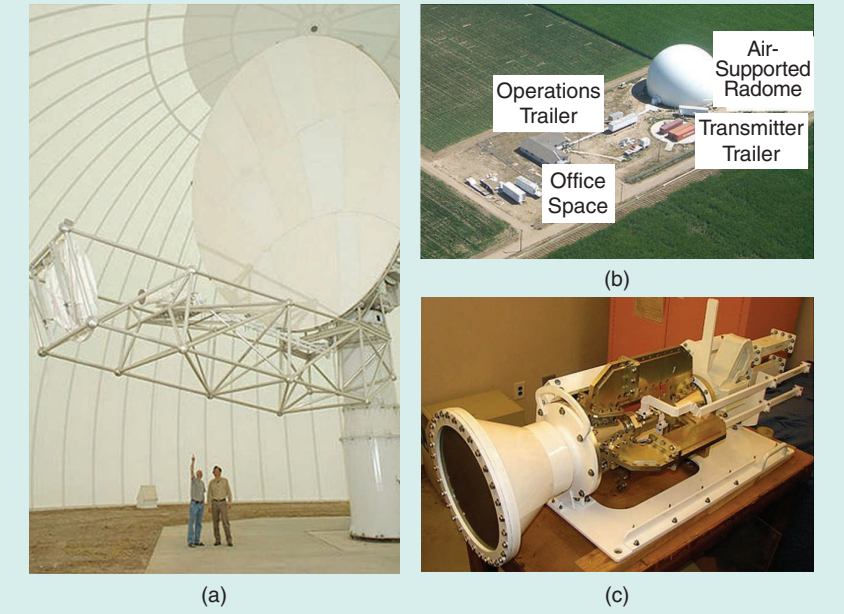

FIGURE 4. The CSU–CHILL radar. (a) The CSU–CHILL dual-offset Gregorian parabolic reflector antenna and positioner system. (b) The CSU–CHILL antenna inflatable radome and transmitter and operations trailers. (c) The dual-polarization (h and v), dual-frequency (S and X bands) horn antenna feed for the reflector antenna system in (a), with the output of a magnetron transmitter split to enable the simultaneous radiation of both h and v polarized electromagnetic waves [43], [47], [48].

With this, larger precipitation particles can appear—at the same time and within the same observation—to the radar as electrically small, i.e., in the Rayleigh regime (at 3 GHz), and as of a size comparable to the wavelength (at 9 GHz), where the elements of larger particles (relative to the wavelength) scatter with different phases, potentially producing large variances in the backscatter at each polarization. Rayleigh and non-Rayleigh scattering behaviors, respectively, at the two frequencies, can be compared, providing additional information about precipitation. In addition, propagation through rain, snow, and hail at different frequencies undergoes various attenuations, which can also be used for observation and analysis. Note that differential attenuation at each polarization and differential phase shifts during propagation also provide information on the particle shapes, sizes, and number distributions [14]. Overall, dual-wavelength scattering and propagation information, provided by dual-wavelength radars, has many uses in atmospheric science research and meteorological practice [48], [49].

APPLICATION OF POLARIMETRIC RADARS IN MASCRAD SNOW FIELD CAMPAIGN

MASCRAD winter field experiments were conducted in Colorado, from 2014 to 2017. The campaign featured combined radar and in situ observations and analyses of geometrical, microphysical, and scattering properties of snowfall [50]–[56], as depicted in Figure 6. The primary radar for the campaign was CSU–CHILL (Figure 4), with added observations from

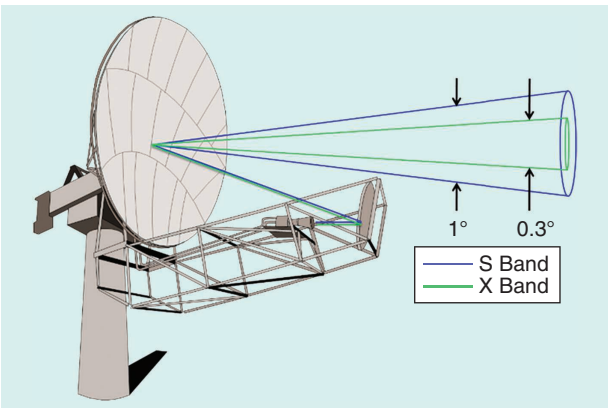

FIGURE 5. The radiation patterns at the S and X bands of the CSU–CHILL radar antenna in Figure 4(a) [43], [48].

National Center for Atmospheric Research (NCAR) SPOL radar, which is a state-of-the-art, dual-polarization S-band weather research radar [57]. In situ surface instruments were placed within a wind shield at a field site at Easton Airport, near Greeley, Colorado (Figure 6) [50]. The instrumentation included a multiangle snowflake camera (MASC) [51], [52], 2D video disdrometer (2DVD) [50], [55], and mobile sounding equipment for launching radiosondes into the atmosphere [50].

The location of the MASCRAD site relative to the CSU–CHILL and NCAR SPOL radars is provided in Figure 7; it is at a 171.3° azimuth and 12.92-km range from CSU–CHILL. When selecting the surface instrumentation site, our principal goal was to minimize the influence of ground clutter for the operation of CSU–CHILL as our primary radar [50]. The objective was to facilitate the lowest feasible elevation angles of the radar, enabling the antenna beam (in Figure 5) to be as close as possible to the measurement volumes of the surface-based optical instruments at the site. This maximally reduced the vertical separation between the radar pulse sample volume and the MASC and 2DVD and thus made the measurements of the snow by the optical instruments maximally relevant with respect to the observations of the snow in the radar volume aloft. On the other hand, when the elevation angle is too low, meteorological data collected by the radar become contaminated due to ground clutter.

The MASCRAD site, being on a ridge, is ~32 m higher than the CSU–CHILL base, and the South Platte River valley, with reduced terrain heights, is located in between (Figure 8). This supported clutter-free data collection by the radar at antenna beam elevations down to only 0.9° across the instrumentation site. At the ~13-km range (Figure 7) and 0.9° elevation, the main beam of the CSU–CHILL antenna at the X band, being 0.33° wide (Figure 5), illuminated a radar volume between 150 and 224 m above ground level at the site.

Prescribed sequences of high-spatial-and-temporal-resolution CHILL radar scans focusing on the MASCRAD field site (Figure 6) were run, with a typical sequence including a 50° plan position indicator (PPI) volume sweep with the lowest clutter-free elevation angle of 0.9°. Two range height indicator (RHI) scans on azimuths that bordered the Easton site, at 171 and 172°, were also done [50], [56]. This combination of PPI and RHI scans was repeated at 3-min intervals, and a cycle was usually augmented by three fixed pointing beam measurements with a dwell time of 20 s each.

Additionally, the KFTG WSR-88D radar located near Denver (Colorado) and KCYS WSR-88D radar in Cheyenne (Wyoming), which are part of the NWS Next-Generation Radar (NEXRAD) dual-polarization, S-band Doppler weather radar network (Figure 3), were used as valuable secondary resources for validating and complementing CSU–CHILL and SPOL data.

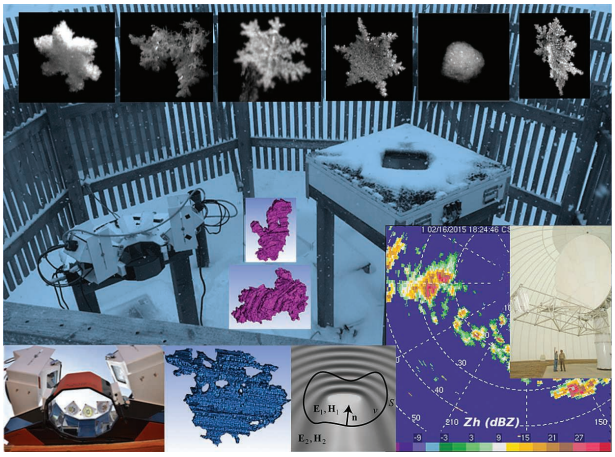

FIGURE 6. The MASCRAD snow field campaign [50]. The CSU-improved multiangle snowflake camera (MASC) (photos on the left) is used to capture high-resolution images of snowflakes in a free fall (images at the top), along with their fall speeds [51], [52]. A visual hull method is employed for the 3D shape reconstruction of precipitation particles by processing the images captured by the MASC (meshes at the center and bottom) [51]. Polarimetric scattering (Figure 1) analysis based on the method of moments (MoM) in conjunction with the surface integral equation (SIE) formulation (sketch at the bottom) is carried out on the reconstructed meshes [53]. A 2D video disdrometer (2DVD) (photo on the right), collocated with the MASC, provides 2D contours of a particle and the fall speed and other important parameters [50], [55]. We use the fall speed as well as environmental conditions measured at the instrumentation site to estimate the particle mass (Böhm's method) and then the effective dielectric constant of the particles, based on a Maxwell–Garnet formula [51]. We develop geometrical, microphysical, and scattering models of natural snowflakes by using the MASC, 2DVD, visual hull, and MoM–SIE and tie them with CSU–CHILL radar (Figure 4) observations (bottom right) [50], [55], [56]. dBZ: decibels relative to *Z*.

ILLUSTRATIVE EXAMPLES OF POLARIMETRIC RADAR OBSERVATIONS FROM COLORADO AND ALABAMA

The first example of polarimetric weather radar observations, presented in Figure 9, is the vertical profile of CSU–CHILL radar (Figure 4) S-band data at 19:32 UTC on 16 February 2015, over the MASCRAD field site (Figures 6–8) during a snow event with a documented graupel shower [55]. Details of obtaining the radar height profile data are given in [55]. We

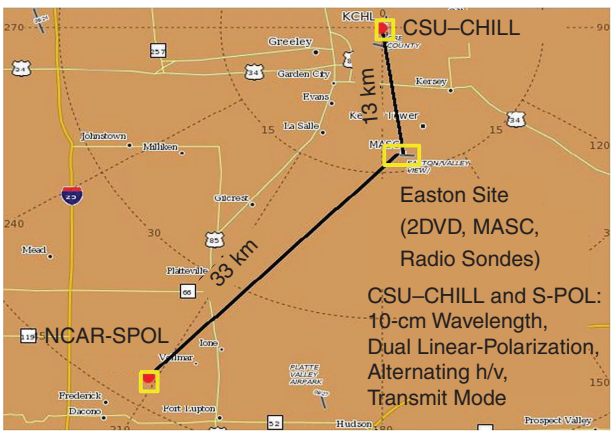

FIGURE 7. MASCRAD radar observations were made by two ~10-cm-wavelength, dual-polarization systems: CSU–CHILL and NCAR SPOL, located, respectively, ~13 and ~33 km from the surface instrumentation site (in Figure 6). The CSU–CHILL radar includes an X-band system as well and can operate in dual-frequency mode (Figure 4) [50].

observe from the figure that the measured horizontal reflectivity and differential reflectivity near the surface and lower than 2 km were roughly $Z_h \approx 25$ dB relative to Z (dBZ) (rather high) and $Z_{dr} \approx -0.2$ dB (slightly negative), respectively, and then Z_h decreased, and Z_{dr} increased rapidly, with a height from 2 km upward to, for instance, $Z_{dr} \approx 0.8$ dB (positive) and very low Z_h levels around 3.5 km. Such a vertical profile with negative Z_{dr} values in the high-Z_h areas along a vertical column is indicative of graupel particles of a lump type located below 2 km. On the other hand, the positive Z_{dr} and low Z_h at higher altitudes signify the likely predominance of pristine crystals.

The conversion of pristine crystals to graupel particles between the two regions occurred via riming, an ice crystal growth process characterized by supercooled water droplets being collected at the surface of ice crystals. Particle riming represents an important microphysical process that affects the particle fall speed and microwave backscattering properties measured by a radar [54], [56]. This conclusion about the transformation of pristine crystals into graupel by riming is supported by meteorological analysis of sounding data. Moreover, images of particles collected by the MASC and 2DVD at the surface (Figure 6) showed graupel particles, as in Figure 10, where the measured fall speeds and densities of the particles were typical for graupel as well. Finally, microwave backscatter calculations confirmed slightly negative Z_{dr} values, as did those measured by the radar, resulting from the shapes and orientations of graupel particles observed by the MASC and 2DVD [55].

The second example is a major snow band passing across the MASCRAD field site on 21 February 2015, with very high reflectivity (Z_h) values in excess of 30 dBZ [50]. In the lowest ~1 km from the surface, the differential reflectivity (Z_{dr}) was consistently near 0 dB. Characteristic MASC images are located in the insets of Figure 11. These were typically relatively large-diameter rimed aggregates, and the concentrations of images (and particles) were high, which is consistent with the observed high Z_h values. However, these aggregates exhibited irregular shapes and orientations, which explains measured Z_{dr} values near 0 dB. Figure 11 compares radar Z_{dr} and LDR values observed in the graupel shower and snow band on 16 and 21 February, respectively. Both events exhibit Z_{dr} encompassing small positive and negative values (around 0 dB), with the histogram of the 16 February case, with graupel particles per MASC data, being distinctly skewed to the negative Z_{dr} range. On the other hand, the 21 February case shows slightly higher LDR levels, which can be attributed to the large aggregates having more irregular shapes that are farther from the sphere, as recorded by the MASC in the snow band [50].

The third example is a dissipating light snow area event of 3 March 2015 at and around the MASCRAD site, with low reflectivity (single-digit, positive Z_h values) and markedly positive Z_{dr} (exceeding +5 dB at times), as shown in Figure 12 [50]. A low Z_h indicates minor concentrations of particles (provided that the particles are not tiny), and when the particles are in small numbers, they collide and aggregate less frequently. With minimal "aggregational" collisions occurring, the Z_{dr} near the ground is evidently positive, which is intrinsic for individual crystals. In other words, the pristine, single crystals growing at higher altitudes with cooler temperatures maintain their flat aspect

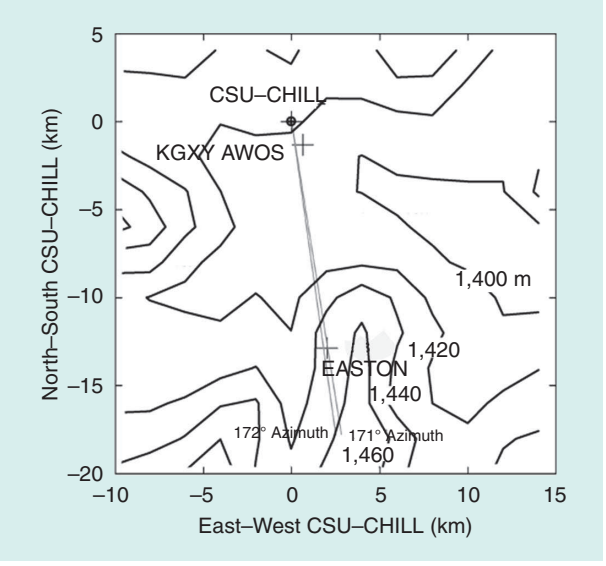

FIGURE 8. The terrain height contours (in meters above mean sea level) around the CSU–CHILL radar and MASCRAD field site at Easton, used for the evaluation of ground clutter between the radar and instrumentation location. The radar azimuths bordering the site (in Figure 6) are in gray [56]. AWOS: automated weather-observing system.

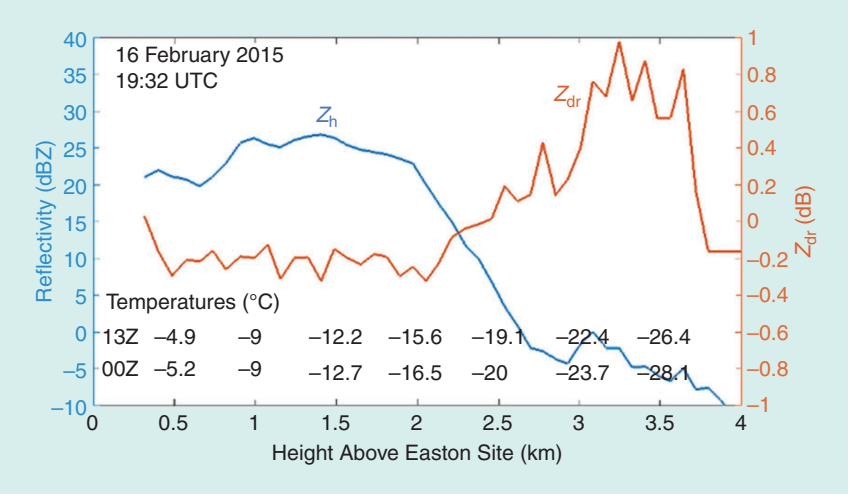

FIGURE 9. The height profiles of horizontal reflectivity (Z_h) and differential reflectivity (Z_{dr}) (Figure 1) using the CSU–CHILL radar (Figure 4) S-band channel averaged across a ±0.25-km range interval of the MASCRAD field site (Figures 6–8) during a graupel shower on 16 February 2015. Temperatures from the MASCRAD sounding (upper row) and NWS Denver sounding (lower row) are given at 0.5-km height intervals along the abscissa [55].

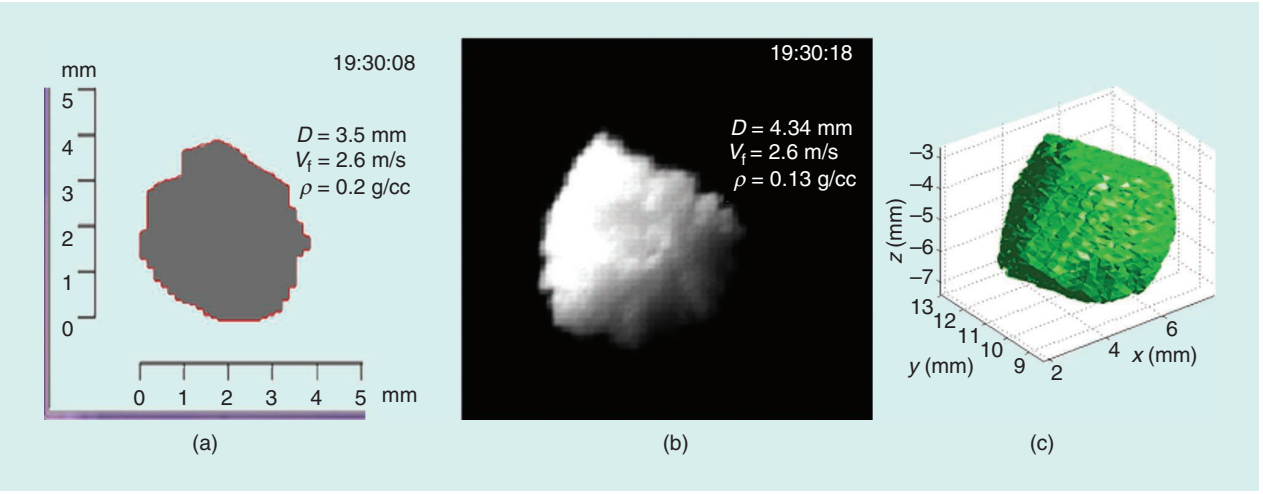

FIGURE 10. Sample graupel images from the (a) 2DVD (Figure 6) and (b) MASC (Figure 6) collected at the MASCRAD field site (Figures 6–8) at ~19:30 UTC on 16 February 2015. The equivolume spherical diameter (D), fall speed, and density of the particles measured by the instruments are also shown. (c) The visual hull 3D shape reconstruction (Figure 6) based on the five MASC images of the particle in (b).

ratios and positive Z_{dr} as they descend, with infrequent collisions, to the ground. Indeed, individual crystal components are more readily apparent in the selected MASC images in the insets of Figure 12 when compared, for example, to the heavily rimed aggregates of the 21 February snow band case in Figure 11, indicating that there may be at least a mixture of pristine particles and aggregates that can produce the observed radar values [50].

The fourth example is a rain event that occurred on 25 December 2009 in Huntsville, Alabama, with C-band polarimetric observations by ARMOR radar, given in Figure 13(a) [58], and ground measurements by a 2DVD (Figure 6) [59]. 2DVD measurements showed that a significant fraction of the raindrops was undergoing asymmetric mode oscillations, depicted in Figure 13(b), which were attributed to frequent and sustained drop collisions [60]. Scattering calculations for 10,233 larger asymmetric drops during a 100-min period were performed using the method of moments (MoM) for solving surface integral equations (SIEs) [53], [59] based on drop 3D shapes reconstructed from the collected 2DVD images, as illustrated in

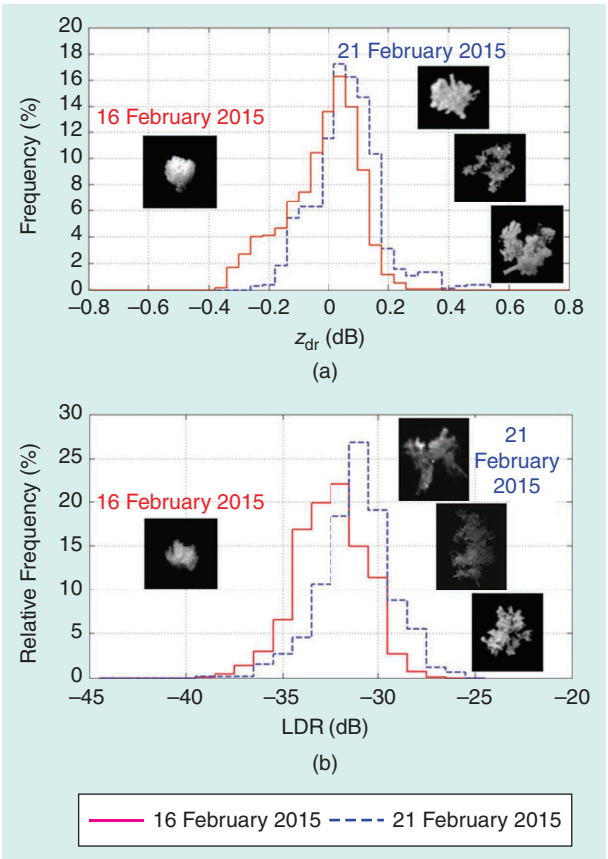

FIGURE 11. The CSU–CHILL radar-measured (Figure 4) S-band (a) Z_{dr} and (b) LDR (see the "Radar Polarimetry: Need and Principles" section) histograms for the 16 February graupel (Figures 9 and 10) and 21 February 2015 snow band cases at the MASCRAD field site (Figures 6–8) (data from [50]). Sample MASC (Figure 6) images captured during each of the events are also shown.

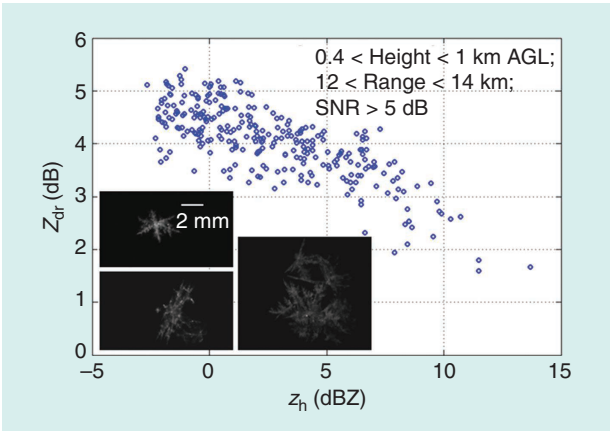

FIGURE 12. The Z_h-versus-Z_{dr} (Figure 1) scatterplot measured by the CSU–CHILL radar (Figure 4) at the S band during a positive Z_{dr} in dissipating light snow area event on 3 March 2015 at the MASCRAD field site (Figure 6). Selected MASC images are shown as well [50]. AGL: above ground level; SNR: signal-to-noise ratio.

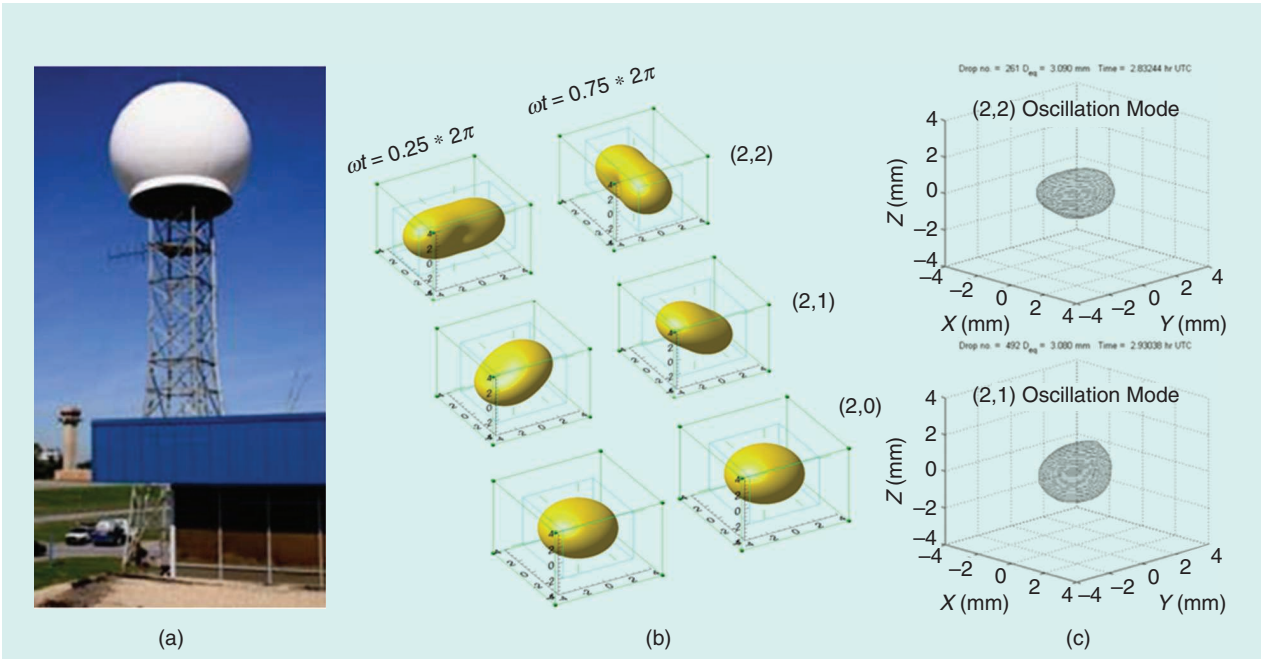

FIGURE 13. (a) The ARMOR C-band (5.625-GHz), polarimetric Doppler weather radar operated by the University of Alabama in Huntsville and National Space Science and Technology Center, Huntsville [58]. (b) 3D views of the three fundamental oscillation modes, for two phases of the oscillation cycle, of asymmetric raindrops resulting from collision-induced drop oscillations (all units are in millimeters) [60]. (c) 3D shapes of two raindrops in different oscillation modes, reconstructed using two perpendicular drop contours from 2DVD (Figure 6) measurements [61] during a rain event on 25 December 2009 in Huntsville. The 2DVD site is at a ~15-km range from the radar, the lowest elevation angle of the radar antenna is 1.3°, and the radar resolution volume is at ~340 m from the surface at this elevation [62].

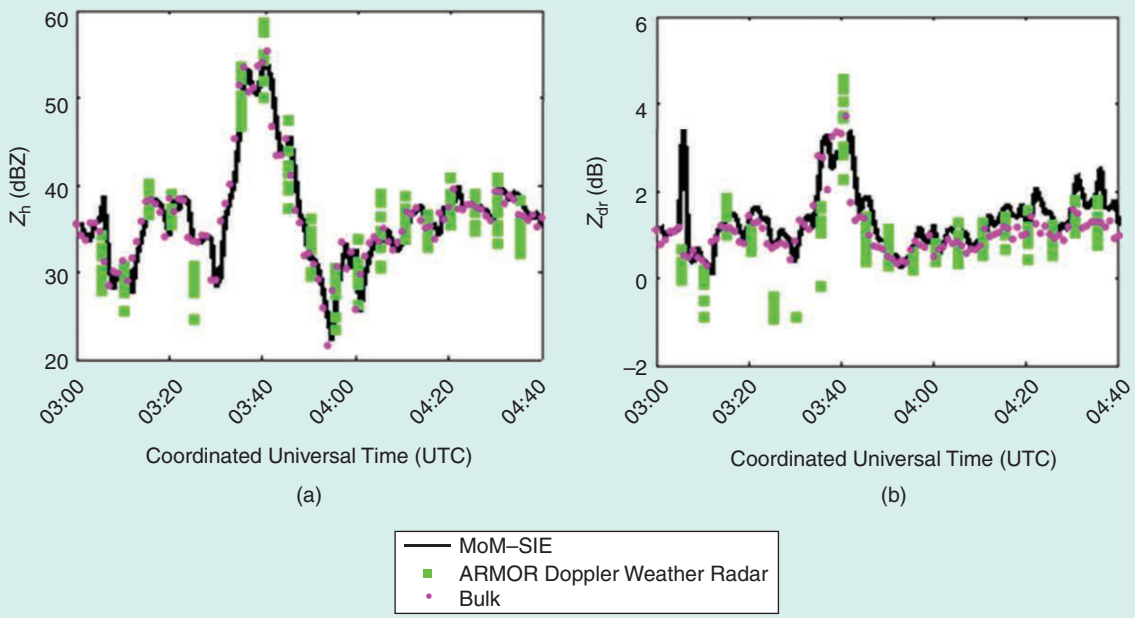

FIGURE 14. The scattering computations and radar measurements at 5.625 GHz of (a) reflectivity (Z_h) and (b) differential reflectivity (Z_{dr}) (Figure 1) through a period of 100 min during the 25 December 2009 rain event in Huntsville, Alabama [59]. The measurements are by the dual-polarization, C-band ARMOR radar [Figure 13(a)]. The scattering calculations are performed using the MoM–SIE technique (Figure 6) based on integration during each 1-min period, using the MoM–SIE drop-by-drop method (for scattering amplitudes of individual drops), with MoM–SIE models reconstructed from 2DVD images [Figure 13(c)], as well as by using the T-matrix scattering code, referred to as the *bulk method* [59].

Figure 13(c) [61]. Figure 14 shows excellent agreement between polarimetric scattering calculations on a drop-by-drop basis at the C band [59] and the radar measurements, which is a remarkable result, given a large volume at a considerable height of radar-observed raindrops compared to ground observations within a disproportionately smaller measurement volume by the 2DVD [62].

CONCLUSIONS

This article explained the principles and applications of polarimetric Doppler weather radars, including some historical asides, with special attention to the CSU–CHILL radar, its components and capabilities, and its setup and role in MASCRAD winter field experiments in Colorado, from 2014 to 2017. Radar polarimetry is a key enabling methodology and technology of radar meteorology, which, in turn, is absolutely essential for accurate and reliable weather forecasts.

The article discussed several illustrative examples of polarimetric weather radar operations and observations and scattering calculations at different frequencies and in different climates. Dual-polarization radar signatures were analyzed in relation to images and measurements by optical instrumentation, namely, the MASC and 2DVD, on the ground. We presented three MASCRAD snowfall cases featuring widely differing meteorological settings that involved contrasting snowflake forms and compositions, such as graupel, heavily rimed aggregates, and pristine crystals. These contrasting snowflake classes strongly influenced S-band polarimetric radar observables, measured by the CSU–CHILL radar, which were used to characterize precipitation and its impacts in various cases. This included the correlation of radar measurements with MASC and 2DVD images and a comparison of the results from different cases. We presented a comparative study of dual-polarization radar measurements at the C band of rainfall, by the ARMOR radar in Alabama, and the associated polarimetric scattering calculations, by the MoM–SIE method, of 2DVD shape-reconstructed asymmetric raindrops resulting from collision-induced, mixed-mode drop oscillations.

As an additional example, which is a part of current and future analysis in the international community, Figure 15 illustrates the use of polarimetric radars within field experiments conducted in conjunction with the 2018 Winter Olympics, in South Korea, namely, International Collaborative Experiments for Pyeongchang 2018 Olympic and Paralympics Winter Games (ICE-POP 2018). Figure 15 includes the list and locations of ICE–POP 2018 radars, where the sites were selected to minimize beam blockage due to the mountainous terrain over the supersites with ground instrumentation enabling radar measurements within 200–400 m above the surface. The analyses of radar and surface data collected during ICE–POP 2018 are ongoing.

Polarimetric scattering observables (e.g., Z_{dr} and LDR) and dual-polarization radar measurements and calculations of scattering from precipitation are a vital prerequisite for a detailed understanding of microphysical properties of snow, rain, and hail particles and for radar-based quantitative precipitation estimation. They are crucial for enhancing our understanding of cloud processes and the resulting precipitation production and snow/water accumulation, and they feed directly into the development, validation, improvement, and use of numerical models for cloud and precipitation simulations, forecasting, and regional climate projections.

Overall, the goals of the article were to introduce radar polarimetry, which generally is a less widely known concept of radar technologies and applications, to describe the electromagnetic and engineering background of dual-polarization radar, show how invaluable its use and impact are in meteorology and atmospheric science, and discuss some fascinating polarimetric radar signatures in snow and rain storms. However, polarimetric Doppler radar can be used for dual-polarization measurements of scattering from nonprecipitation particles and objects as well, with a multitude of potential applications in the detection, evaluation, and analysis of various targets [64], [65], which, of course, do not need to be small at all. Examples include the use of polarimetric radar for

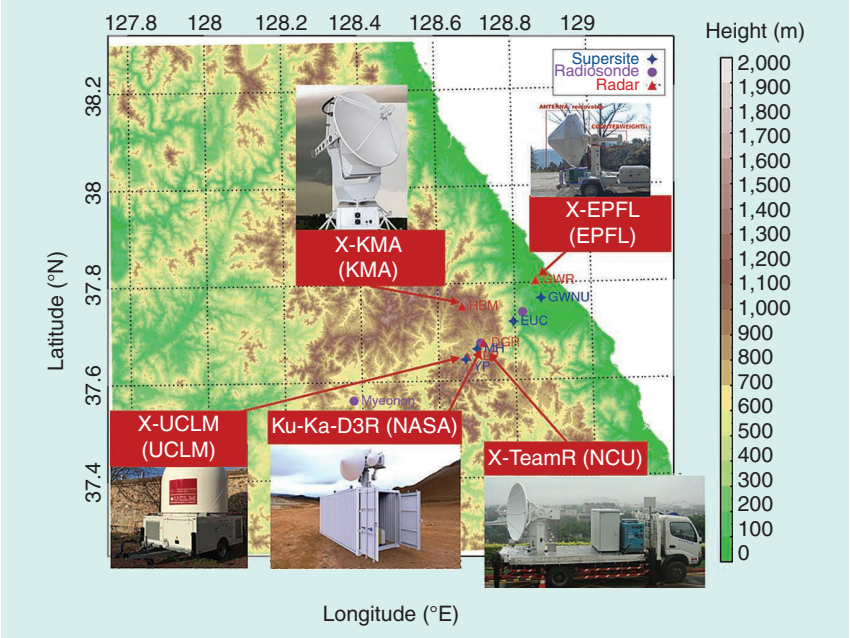

FIGURE 15. The unique composition of radars for the International Collaborative Experiments for Pyeongchang 2018 Olympic and Paralympic Winter Games (ICE-POP 2018), South Korea: the location of four X-band, dual-polarization Doppler radars (from four institutions/agencies in Asia and Europe), X-KMA, X-EPFL, X-UCLM, and X-TeamR, owned by Korea Meteorological Administration (KMA), South Korea, Federal Institute of Technology in Lausanne (EPFL), Switzerland, University of Castilla–La Mancha (UCLM), Spain, and National Central University (NCU), Taiwan, respectively, and NASA's dual-polarization, dual-wavelength (K_u and K_a)-band radar (D3R) [49], [63] across 2018 Winter Olympics venues, in Pyeongchang region on Korean peninsula.

health-care sensing [42] as well as dual-polarization radar observations of biological targets (e.g., insects, birds, and bats) [66]–[68], smoke and ash from fires and volcanoes [69]–[71], tornadic debris [72], ground and sea clutter [73], [74], and military chaff [75]. Finally, there are significant improvements in radar polarimetry coming from advances in signal processing techniques and architectures, for example, a multiple-input, multiple-output radar with instantaneous radar polarimetry [76].

ACKNOWLEDGMENTS

This work was supported by the U.S. National Science Foundation, under grants AGS-1344862, AGS-1431127, and AGS-2029806, and NASA Precipitation Measurements Mission grant NNX16AE43G. The author would like to thank his collaborators and students: Prof. V.N. Bringi, Patrick Kennedy, Dr. Merhala Thurai, Dr. Gwo-Jong Huang, Dr. Andrew J. Newman, Prof. GyuWon Lee, Dr. John Hubbert, Cameron Kleinkort, Dr. Sanja B. Manić, Dr. Elene Chobanyan, and Adam Hicks. The author is also grateful to Prof. Steven A. Rutledge, scientific director, CSU–CHILL National Radar Facility, for providing the presentation of [43], from which Figures 1, 2, 4, and 5 were adapted, and Prof. GyuWon Lee, principal investigator, ICE–POP 2018, for providing Figure 15.

AUTHOR INFORMATION

Branislav M. Notaroš (notaros@colostate.edu) is a professor and University Distinguished Teaching Scholar at Colorado State University, Fort Collins, Colorado, 80523, USA. He is the author of several books and recipient of 10 major national and international awards for research and teaching/education. He is a Fellow of IEEE.

REFERENCES

[1] D. Atlas, Ed. *Radar in Meteorology*. Boston, MA, USA: American Meteorological Society, 1990.

[2] J. Leinonen, D. Moisseev, and T. Nousiainen, "Linking snowflake microstructure to multi-frequency radar observations," *J. Geophys. Res.*, vol. 118, no. 8, pp. 3259–3270, 2013, doi: 10.1002/jgrd.50163.

[3] A. J. Heymsfield, S. Y. Matrosov, and N. B. Wood, "Toward improving ice water content and snow-rate retrievals from radars. Part I: X and W bands, emphasizing CloudSat," *J. Appl. Meteor. Climatol.*, vol. 55, no. 9, pp. 2063–2090, 2016, doi: 10.1175/JAMC-D-15-0290.1.

[4] R. Lhermitte, "Application of pulse Doppler radar technique to meteorology," *Bull Amer. Meteor. Soc.*, vol. 47, no. 9, pp. 703–711, 1966, doi: 10.1175/1520-0477-47.9.703.

[5] R. J. Doviak and D. S. Zrnic, *Doppler Radar and Weather Observations*, 2nd ed. San Diego, CA, USA: Academic, 1993.

[6] V. N. Bringi and V. Chandrasekar, *Polarimetric Doppler Weather Radar: Principles and Applications*. Cambridge, U.K.: Cambridge Univ. Press, 2001.

[7] A. Ryzhkov and D. S. Zrnic, *Radar Polarimetry for Weather Observations*. Cham, Switzerland: Springer-Verlag, 2019.

[8] G. Zhang, *Weather Radar Polarimetry*. Boca Raton, FL, USA: CRC Press, 2017.

[9] V. Bringi and D. Zrnic, "Polarization weather radar development from 1970–1995: Personal reflections," *Atmosphere*, vol. 10, no. 11, p. 714, 2019, doi: 10.3390/atmos10110714.

[10] R. M. Rauber and S. W. Nesbitt, *Radar Meteorology: A First Course*. Hoboken, NJ, USA: Wiley, 2018.

[11] A. Kostinski and W. Boerner, "On foundations of radar polarimetry," *IEEE Trans. Antennas Propag.*, vol. 34, no. 12, pp. 1395–1404, 1986, doi: 10.1109/TAP.1986.1143771.

[12] E. M. Griffin, T. J. Schuur, A. V. Ryzhkov, H. D. Reeves, and J. C. Picca, "A polarimetric and microphysical investigation of the northeast blizzard of 8–9 February 2013," *Weather Forecast.*, vol. 29, no. 6, pp. 1271–1294, 2014, doi: 10.1175/WAF-D-14-00056.1.

[13] A. V. Ryzhkov and D. S. Zrnic, "Discrimination between rain and snow with a polarimetric radar," *J. Appl. Meteor.*, vol. 37, no. 10, pp. 1228–1240, 1998, doi: 10.1175/1520-0450(1998)037<1228:DBRASW>2.0.CO;2.

[14] M. Thurai, E. Chobanyan, V. N. Bringi, and B. M. Notaros, "Large raindrops against melting hail: Calculation of specific differential attenuation, phase and reflectivity," *Electron. Lett.*, vol. 51, no. 15, pp. 1140–1142, 2015, doi: 10.1049/el.2015.1564.

[15] A. V. Ryzhkov, S. E. Giangrande, and T. J. Schuur, "Rainfall estimation with a polarimetric prototype of WSR-88D," *J. Appl. Meteor.*, vol. 44, no. 4, pp. 502–515, 2005, doi: 10.1175/JAM2213.1.

[16] M. Thurai, V. N. Bringi, and W. A. Petersen, "Rain microstructure retrievals using 2-D video disdrometer and C-band polarimetric radar," *Adv. Geosci.*, vol. 20, pp. 13–18, Mar. 2009, doi: 10.5194/adgeo-20-13-2009.

[17] V. N. Bringi, C. R. Williams, M. Thurai, and P. T. May, "Using dual-polarized radar and dual-frequency profiler for DSD characterization: A case study from Darwin, Australia," *J. Atmos. Ocean. Technol.*, vol. 26, no. 10, pp. 2107–2122, 2009, doi: 10.1175/2009JTECHA1258.1.

[18] P. Tabary, G. Vulpiani, J. J. Gourley, A. J. Illingworth, R. J. Thompson, and O. Bousquet, "Unusually high differential attenuation at C band: Results from a two-year analysis of the French trappes polarimetric radar data," *J. Appl. Meteor. Climatol.*, vol. 48, no. 10, pp. 2037–2053, 2009, doi: 10.1175/2009JAMC2039.1.

[19] C. C. Crowe, C. J. Schultz, M. R. Kumjian, L. D. Carey, and W. A. Petersen, "Use of dual-polarization signatures in diagnosing tornadic potential," *Electron. J. Oper. Meteor.*, vol. 13, no. 5, pp. 57–78, 2012.

[20] M. Thurai, V. N. Bringi, L. D. Carey, P. Gatlin, E. Schultz, and W. A. Petersen, "Estimating the accuracy of polarimetric radar-based retrievals of drop size distribution parameters and rain rate: An application of error variance separation using radar-derived spatial correlations," *J. Hydrometeor.*, vol. 13, no. 3, pp. 1066–1079, 2012, doi: 10.1175/JHM-D-11-070.1.

[21] L. D. Carey and W. A. Petersen, "Sensitivity of C-band polarimetric radar–based drop size estimates to maximum diameter," *J. Appl. Meteor. Climatol.*, vol. 54, no. 6, pp. 1352–1371, 2015, doi: 10.1175/JAMC-D-14-0079.1.

[22] C. Sandford, A. Illingworth, and R. Thompson, "The potential use of the linear depolarization ratio to distinguish between convective and stratiform rainfall to improve radar rain-rate estimates," *J. Appl. Meteor. Climatol.*, vol. 56, no. 11, pp. 2927–2940, 2017, doi: 10.1175/JAMC-D-17-0014.1.

[23] J. Straka, D. S. Zrnić, and A. V. Ryzhkov, "Bulk hydrometeor classification and quantification using polarimetric radar data: Synthesis of relations," *J. Appl. Meteor.*, vol. 39, no. 8, pp. 1341–1372, 2000, doi: 10.1175/1520-0450(2000)039<1341:BHCAQU>2.0.CO;2.

[24] D. S. Zrnić, A. Ryzhkov, J. Straka, Y. Liu, and J. Vivekanandan, "Testing a procedure for automatic classification of hydrometeor types," *J. Atmos. Oceanic Technol.*, vol. 18, no. 6, pp. 892–913, 2001, doi: 10.1175/1520-0426(2001)018<0892:TAPFAC>2.0.CO;2.

[25] P. C. Kennedy and S. A. Rutledge, "S-band dual-polarization radar observations of winter storms," *J. Appl. Meteor. Climatol.*, vol. 50, no. 4, pp. 844–858, 2011, doi: 10.1175/2010JAMC2558.1.

[26] G. Zhang, S. Luchs, A. Ryzhkov, M. Xue, L. Ryzhkova, and Q. Cao, "Winter precipitation microphysics characterized by polarimetric radar and video disdrometer observations in central Oklahoma," *J. Appl. Meteor. Climatol.*, vol. 50, no. 7, pp. 1558–1570, 2011, doi: 10.1175/2011JAMC2343.1.

[27] J. Andric, M. R. Kumjian, D. S. Zrnic, J. M. Straka, and V. M. Melnikov, "Polarimetric signatures above the melting layer in winter storms: An observational and modeling study," *J. Appl. Meteor. Climatol.*, vol. 52, no. 3, pp. 682–700, 2013, doi: 10.1175/JAMC-D-12-028.1.

[28] R. Bechini, L. Baldini, and V. Chandrasekar, "Polarimetric radar observations in the ice region of precipitating clouds at C-band and X-band radar frequencies," *J. Appl. Meteor. Climatol.*, vol. 52, no. 5, pp. 1147–1169, 2013, doi: 10.1175/JAMC-D-12-055.1.

[29] M. R. Kumjian, A. V. Ryzhkov, H. D. Reeves, and T. J. Schuur, "A dual-polarization radar signature of hydrometeor refreezing in winter storms," *J. Appl. Meteor. Climatol.*, vol. 52, no. 11, pp. 2549–2566, 2013, doi: 10.1175/JAMC-D-12-0311.1.

[30] M. Schneebeli, N. Dawes, M. Lehning, and A. Berne, "High-resolution vertical profiles of X-band polarimetric radar observables during snowfall in the Swiss Alps," *J. Appl. Meteor. Climatol.*, vol. 52, no. 2, pp. 378–394, 2013, doi: 10.1175/JAMC-D-12-015.1.

[31] R. S. Schrom, M. R. Kumjian, and Y. Lu, "Polarimetric radar signatures of dendritic growth zones within Colorado winter storms," *J. Appl. Meteor. Climatol.*, vol. 54, no. 12, pp. 2365–2388, 2015, doi: 10.1175/JAMC-D-15-0004.1.

[32] G. Skofronick-Jackson *et al.*, "Global precipitation measurement cold season precipitation experiment (GCPEX): For measurement's sake, let it snow," *Bull.*

Amer. Meteor. Soc., vol. 96, no. 10, pp. 1719–1741, 2015, doi: 10.1175/BAMS-D-13-00262.1.
[33] A. Ryzhkov *et al.*, "Quasi-vertical profiles—A new way to look at polarimetric radar data," *J. Atmos. Oceanic Technol.*, vol. 33, no. 3, pp. 551–562, 2016, doi: 10.1175/JTECH-D-15-0020.1.
[34] G. Zhang *et al.*, "Current status and future challenges of weather radar polarimetry: Bridging the gap between radar meteorology/hydrology/engineering and numerical weather prediction," *Adv. Atmos. Sci.*, vol. 36, no. 6, pp. 571–588, 2019, doi: 10.1007/s00376-019-8172-4.
[35] R. J. Hogan, L. Tian, P. R. A. Brown, C. D. Westbrook, A. J. Heymsfield, and J. D. Eastment, "Radar scattering from ice aggregates using the horizontally aligned oblate spheroid approximation," *J. Appl. Meteorol. Climatol.*, vol. 51, no. 3, pp. 655–671, 2012, doi: 10.1175/JAMC-D-11-074.1.
[36] J. Tyynelä, J. Leinonen, C. D. Westbrook, D. Moisseev, and T. Nousiainen, "Applicability of the Rayleigh–Gans approximation for scattering by snowflakes at microwave frequencies in vertical incidence," *J. Geophys. Res. Atmos.*, vol. 118, no. 4, pp. 1826–1839, 2013, doi: 10.1002/jgrd.50167.
[37] R. M. Wakimoto and V. N. Bringi, "Dual-polarization observations of microbursts associated with intense convection: The 20 July storm during the MIST project," *Mon. Weather Rev.*, vol. 116, no. 8, pp. 1521–1539, 1988, doi: 10.1175/1520-0493(1988)116<1521:DPOOMA>2.0.CO;2.
[38] R. J. Hogan, P. R. Field, A. J. Illingworth, R. J. Cotton, and T. W. Choularton, "Properties of embedded convection in warm-frontal mixed-phase cloud from aircraft and polarimetric radar," *Quart. J. Roy. Meteor. Soc.*, vol. 128, no. 580, pp. 451–476, 2002, doi: 10.1256/003590002321042054.
[39] E. Torlaschi and A. R. Holt, "A comparison of different polarization schemes for the radar sensing of precipitation," *Radio Sci.*, vol. 33, no. 5, pp. 1335–1352, 1998, doi: 10.1029/98RS00633.
[40] M. Galletti, D. Huang, and P. Kollias, "Zenith/Nadir pointing mm-wave radars: Linear or circular polarization?" *IEEE Trans. Geosci. Remote Sens.*, vol. 52, no. 1, pp. 628–639, 2014, doi: 10.1109/TGRS.2013.2243155.
[41] B. L. Barge and G. A. Isaac, "The shape of Alberta hailstones," *J. Rech. Atmos.*, vol. 7, pp. 11–20, 1973.
[42] Y. He, C. Gu, H. Ma, J. Zhu, and G. V. Eleftheriades, "Miniaturized circularly polarized Doppler radar for human vital sign detection," *IEEE Trans. Antennas Propag.*, vol. 67, no. 11, pp. 7022–7030, 2019, doi: 10.1109/TAP.2019.2927777.
[43] S. A. Rutledge, *Innovative Radar Research at CSU* (College of Engineering Innovation Series), Denver, CO, USA: Colorado State Univ., CSU Denver Center.
[44] T. A. Seliga and V. N. Bringi, "Potential use of radar differential reflectivity measurements at orthogonal polarizations for measuring precipitation," *J. Appl. Meteor.*, vol. 15, no. 1, pp. 69–76, 1976, doi: 10.1175/1520-0450(1976)015<0069:PUORDR>2.0.CO;2.
[45] E. Udell, "Spring creek flood anniversary: Revisit the deadly night," *The Coloradoan*, Jul. 20, 2017.
[46] The American Meteorological Society, *2012 Remote Sensing Prize Winner Sees Polarimetric Radar Research Go Nationwide*. The Front Page, Boston, MA, USA, Jan. 26, 2012.
[47] V. N. Bringi *et al.*, "Design and performance characteristics of the new 8.5-m dual-offset Gregorian antenna for the CSU–CHILL radar," *J. Atmos. Oceanic Technol.*, vol. 28, no. 7, pp. 907–920, 2011, doi: 10.1175/2011JTECHA1493.1.
[48] F. Junyent *et al.*, "Transformation of the CSU-CHILL radar facility to a dual-frequency, dual-polarization Doppler system," *Bull. Amer. Meteor. Soc.*, vol. 96, no. 6, pp. 975–996, 2015, doi: 10.1175/BAMS-D-13-00150.1.
[49] G.-J. Huang, V. N. Bringi, A. J. Newman, G. Lee, D. Moisseev, and B. M. Notaros, "Dual-wavelength radar technique development for snow rate estimation: A case study from GCPEx," *Atmos. Measure. Techn.*, vol. 12, no. 2, pp. 1409–1427, 2019, doi: 10.5194/amt-12-1409-2019.
[50] B. M. Notaros *et al.*, "Accurate characterization of winter precipitation using multi-angle snowflake camera, visual hull, advanced scattering methods and polarimetric radar," *Atmosphere*, vol. 7, no. 6, pp. 81–111, Jun. 2016, doi: 10.3390/atmos7060081.
[51] C. Kleinkort, G.-J. Huang, V. N. Bringi, and B. M. Notaros, "Visual hull method for realistic 3D particle shape reconstruction based on high-resolution photographs of snowflakes in free fall from multiple views," *J. Atmos. Oceanic Technol.*, vol. 34, no. 3, pp. 679–702, Mar. 2017, doi: 10.1175/JTECH-D-16-0099.1.
[52] G.-J. Huang, C. Kleinkort, V. N. Bringi, and B. M. Notaros, "Winter precipitation particle size distribution measurement by multi-angle snowflake camera," *Atmos. Res.*, vol. 198, pp. 81–96, 2017, doi: 10.1016/j.atmosres.2017.08.005.
[53] E. Chobanyan *et al.*, "Efficient and accurate computational electromagnetics approach to precipitation particle scattering analysis based on higher-order method of moments integral equation modeling," *J. Atmos. Oceanic Technol.*, vol. 32, no. 10, pp. 1745–1758, Oct. 2015, doi: 10.1175/JTECH-D-15-0037.1.
[54] A. Hicks and B. M. Notaros, "Method for classification of snowflakes based on images by a multi-angle snowflake camera using convolutional neural networks," *J. Atmos. Oceanic Technol.*, vol. 36, no. 12, pp. 2267–2282, Dec. 2019, doi: 10.1175/JTECH-D-19-0055.1.
[55] V. N. Bringi, P. C. Kennedy, G.-J. Huang, C. Kleinkort, M. Thurai, and B. M. Notaros, "Dual-polarized radar and surface observations of a winter graupel shower with negative Z_{dr} column," *J. Appl. Meteor. Climatol.*, vol. 56, no. 2, pp. 455–470, Feb. 2017, doi: 10.1175/JAMC-D-16-0197.1.
[56] P. Kennedy, M. Thurai, C. Praz, V. N. Bringi, A. Berne, and B. M. Notaros, "Variations in snow crystal riming and Z_{DR}: A case analysis," *J. Appl. Meteor. Climatol.*, vol. 57, no. 3, pp. 695–707, 2018, doi: 10.1175/JAMC-D-17-0068.1.
[57] J. C. Hubbert *et al.*, "FRONT: The front range observational network testbed," Presented at *92nd AMS Annu. Meeting*, Jan. 22–26, 2012, New Orleans, LA.
[58] W. A. Petersen *et al.*, "The NSSTC ARMOR C-band dual-polarimetric Doppler radar: A tool for integrated remote sensing," in *Proc. Huntsville Simulation Conf.*, International Society for Modeling and Simulation, Huntsville, Alabama, Oct. 26–27, 2005.
[59] S. B. Manic, M. Thurai, V. N. Bringi, and B. M. Notaros, "Scattering calculations for asymmetric raindrops during a line convection event: Comparison with radar measurements," *J. Atmos. Oceanic Technol.*, vol. 35, no. 6, pp. 1169–1180, Jun. 2018, doi: 10.1175/JTECH-D-17-0196.1.
[60] M. Thurai, V. N. Bringi, A. B. Manic, N. J. Sekeljic, and B. M. Notaros, "Investigating rain drop shapes, oscillation modes, and implications for radiowave propagation," *Radio Sci.*, vol. 49, no. 10, pp. 921–932, 2014, doi: 10.1002/2014RS005503.
[61] M. Thurai, S. Manic, M. Schönhuber, V. N. Bringi, and B. M. Notaros, "Scattering calculations at C-band for asymmetric raindrops reconstructed from 2D video disdrometer measurements," *J. Atmos. Oceanic Technol.*, vol. 34, no. 4, pp. 765–776, Apr. 2017, doi: 10.1175/JTECH-D-16-0141.1.
[62] M. Thurai *et al.*, "Toward completing the raindrop size spectrum: Case studies involving 2D-video disdrometer, droplet spectrometer, and polarimetric radar measurements," *J. Appl. Meteor. Climatol.*, vol. 56, no. 4, pp. 877–896, Apr. 2017, doi: 10.1175/JAMC-D-16-0304.1.
[63] M. A. Vega, V. Chandrasekar, J. Carswell, R. M. Beauchamp, M. R. Schwaller, and C. Nguyen, "Salient features of the dual-frequency, dual-polarized, Doppler radar for remote sensing of precipitation," *Radio Sci.*, vol. 49, no. 11, pp. 1087–1105, 2014, doi: 10.1002/2014RS005529.
[64] M. R. Kumjian, "Principles and applications of dual-polarization weather radar. Part I: Description of the polarimetric radar variables," *J. Oper. Meteor.*, vol. 1, no. 19, pp. 226–242, 2013, doi: 10.15191/nwajom.2013.0119.
[65] D. Giuli, "Polarization diversity in radars," *Proc. IEEE*, vol. 74, no. 2, pp. 245–269, 1986, doi: 10.1109/PROC.1986.13457.
[66] D. S. Zrnic and A. V. Ryzhkov, "Observations of insects and birds with a polarimetric radar," *IEEE Trans. Geosci. Remote Sens.*, vol. 36, no. 2, pp. 661–668, 1998, doi: 10.1109/36.662746.
[67] S. M. Bachmann and D. S. Zrnic, "Spectral density of polarimetric variables separating biological scatterers in the VAD display," *J. Atmos. Oceanic Technol.*, vol. 24, no. 7, pp. 1186–1198, 2007, doi: 10.1175/JTECH2043.1.
[68] S. M. Bachmann and D. S. Zrnic, "Suppression of clutter residue in weather radar reveals birds' corridors over urban area," *IEEE Geosci. Rem. Sens. Lett.*, vol. 5, no. 2, pp. 128–132, 2008, doi: 10.1109/LGRS.2008.915601.
[69] V. M. Melnikov, D. S. Zrnic, R. M. Rabin, and P. Zhang, "Radar polarimetric signatures of fire plumes in Oklahoma," *Geophys. Res. Lett.*, vol. 35, no. 14, p. L14815, 2008, doi: 10.1029/2008GL034311.
[70] V. M. Melnikov, D. S. Zrnic, R. M. Rabin, and P. Zhang, "Polarimetric radar properties of smoke plumes: A model," *J. Geophys. Res.*, vol. 114, p. D21204, Nov. 2009, doi: 10.1029/2009JD012647.
[71] T. A. Jones, S. A. Christopher, and W. Petersen, "Dual-polarization radar characteristics of an apartment fire," *J. Atmos. Oceanic Technol.*, vol. 26, no. 10, pp. 2257–2269, 2009, doi: 10.1175/2009JTECHA1290.1.
[72] D. J. Bodine, M. R. Kumjian, R. D. Palmer, P. L. Heinselman, and A. V. Ryzhkov, "Tornado damage estimation using polarimetric radar," *Weather Forecasting*, vol. 28, no. 1, pp. 139–158, 2013, doi: 10.1175/WAF-D-11-00158.1.
[73] M. W. Long, *Radar Reflectivity of the Land and Sea*, 3rd ed. Norwood, MA, USA: Artech House, 2001, p. 534.
[74] D. S. Zrnić, V. M. Melnikov, and A. V. Ryzhkov, "Correlation coefficients between horizontally and vertically polarized returns from ground clutter," *J. Atmos. Oceanic Technol.*, vol. 23, no. 3, pp. 381–394, 2006, doi: 10.1175/JTECH1856.1.
[75] D. S. Zrnic and A. V. Ryzhkov, "Polarimetric properties of chaff," *J. Atmos. Oceanic Technol.*, vol. 21, no. 7, pp. 1017–1024, 2004, doi: 10.1175/1520-0426(2004)021<1017:PPOC>2.0.CO;2.
[76] S. D. Howard, A. R. Calderbank, and W. Moran, "A Simple signal processing architecture for instantaneous radar polarimetry," *IEEE Trans. Inf. Theory*, vol. 53, no. 4, pp. 1282–1289, 2007, doi: 10.1109/TIT.2007.892809.